Fluorescence Quenching Nanoprobes Dedicated to In Vivo Photoacoustic Imaging and High-Efficient Tumor Therapy in Deep-Seated Tissue

Huan Qin, Ting Zhou, Sihua Yang, and Da Xing**

***P**hotoacoustic imaging (PAI) and photoacoustic (PA) therapy have promising applications for treating tumors. It is known that the utilization of high-absorption-coefficient probes can selectively enhance the PAI target contrast and PA tumor therapy efficiency in deep-seated tissue. Here, the design of a probe with the highest availability of optical-thermo conversion by using graphene oxide (GO) and dyes via π–π stacking interactions is reported. The GO serves as a base material for loading dyes and quenching dye fluorescence via fluorescence resonance energy transfer (FRET), with the one purpose of maximum of PA efficiency. Experiments verify that the designed fluorescence quenching nanoprobes can produce stronger PA signals than the sum of the separate signals generated in the dye and the GO. Potential applications of the fluorescence quenching nanoprobes are demonstrated, dedicating to enhance PA contrast of targets in deep-seated tissues and tumors in living mice. PA therapy efficiency both in vitro and in vivo by using the fluorescence quenching nanoprobes is found to be higher than with the commonly used PA therapy agents. Taken together, quenching dye fluorescence via FRET will provide a valid means for developing high-efficiency PA probes. Fluorescence quenching nanoprobes are likely to become a promising candidate for deep-seated tumor imaging and therapy.*

1. Introduction

Photoacoustic imaging (PAI) overcomes the optical diffusion limit and provides deeper tissue imaging with high spatial resolution by integrating optical excitation with ultrasonic detection on the photoacoustic (PA) effect.[1–5] Various endogenous chromophores can serve as PAI contrast agents, enabling brain function study, tumor microcirculation visualization, and atherosclerotic plaque identification.[6–12] However, in most cases, intrinsic biomarkers of many diseases (e.g., cancer) cannot generate PA signals by themselves after laser excitation. Using exogenous PA probes to stain PAI-invisible biomarkers is effective at fully utilizing PAI's potential at a depth and spatial resolution and it ultimately accurately detects these diseases in living subjects.

As an emerging cancer therapy, PA therapy utilizes probes' PA effects to target and selectively destroy cancer cells with minimal normal cell interaction and anticancer drug resistance.[13–15] PA probes with high light-to-acoustic conversion efficiency can generate effective PA wave even when irradiated by a low-energy pulsed laser. Generally, light energy is exponential decay with increasing tissue depth. Utilizing high-efficiency PA probes will be helpful for enhancing imaging contrast and therapy efficiency in deeper tissue. Numerous PA near-infrared probes such as metallic nanoparticles, semiconducting polymer nanoparticles, fluorescent dyes, carbon nanotubes, and graphene oxide (GO) have been applied in PAI to detect tumors, lymph nodes, and

Dr. H. Qin, Dr. T. Zhou, Prof. S. Yang, Prof. D. Xing
MOE Key Laboratory of Laser Life Science
and Institute of Laser Life Science
College of Biophotonics
South China Normal University
Guangzhou 510631, China
E-mail: yangsh@scnu.edu.cn; xingda@scnu.edu.cn

DOI: 10.1002/smll.201403395

inflammation.[16–38] However, these probes have certain limitations and must be improved before they are widely applied in PA imaging and PA therapy. For example, gold nanorods and nanoshells are susceptible to laser-induced deformation, in which their imaging or therapy efficiency declines.[39–41] Fluorescent dyes with spectral selectivity and strong absorption characteristics in a specific wavelength range have attracted researchers' attention for use in PAI and PA therapy.[15,27–29] The absorbed light energy of fluorescent dyes mostly decays the same radioactive way as fluorescence, which affects the light-to-acoustic conversion efficiency. Carbon nanotubes and GO both have a relatively low absorption coefficient in the near infrared region. de la Zerda et al. presented the two high-absorption-coefficient probes including indocyanine green dye-enhanced single walled carbon nanotube (SWNT) and QSY_{21}-enhanced SWNT. Both contrast agents gave a markedly 300 times higher PA contrast in living tissues than previously reported SWNTs, leading to subnanomolar sensitivities.[18–20,30] However, they did not discuss in detail SWNT-dye's PA enhancement mechanism about fluorescence quenching.

New methods are required to develop a PA probe with highest availability of optical-to-acoustic conversion for PAI and PA therapy. Notably, PA wave generation energy arises from nonradiative energy.[1–5,20] Then, the optical-acoustic conversion of fluorescent dyes can be enhanced by increasing the proportion of nonradiative energy or nonradiative quantum yield. Akers et al. demonstrated that quenching the fluorescence of pyrrolopyrrole cyanine in the perfluorocarbon nanoparticles resulted in this part of absorbed light converting to heat,[20] which ultimately improved PA contrast through more efficient thermal expansion. Increasing the proportion of fluorescent dyes' nonradiative energy rather than enhancing the materials' optical absorption coefficient may provide a valid means for developing high-efficiency PA probes.

Herein, we developed dye-coated GO (GO-dyes) probes to enhance PAI contrast and PA therapy efficiency via fluorescence quenching on fluorescence resonance energy transfer (FRET). In FRET, a donor fluorophore is excited by the incident light and the excited state energy can be transferred from the donor to an acceptor molecule in close proximity.[42,40] If the acceptor is a nonfluorescent chromophore, the donor fluorophore fluorescence is quenched and the absorbed energy transferred from the donor will be released mostly in the form of nonradiative energy. GO with an extremely low quantum yield reportedly functions as an acceptor that efficiently quenches the fluorescence of dyes in close proximity.[43–46] GO also possesses an ultra-large specific surface area on a per mass basis, allowing dyes with benzene ring structures to attach to GO via π–π stacking interactions.[47–52] The attached dye molecules on GO can selectively absorb light energy due to their narrow absorption spectral profile. GO efficiently quenches the dye fluorescence via FRET between the dyes and GO, enabling the absorbed light energy to be converted to thermal energy. With a pulse laser, the absorbed light energy of GO-dyes would efficiently convert to acoustic waves via the PA effect (**Figure 1**). This ultimately improved PA contrast through more efficient thermal expansion.

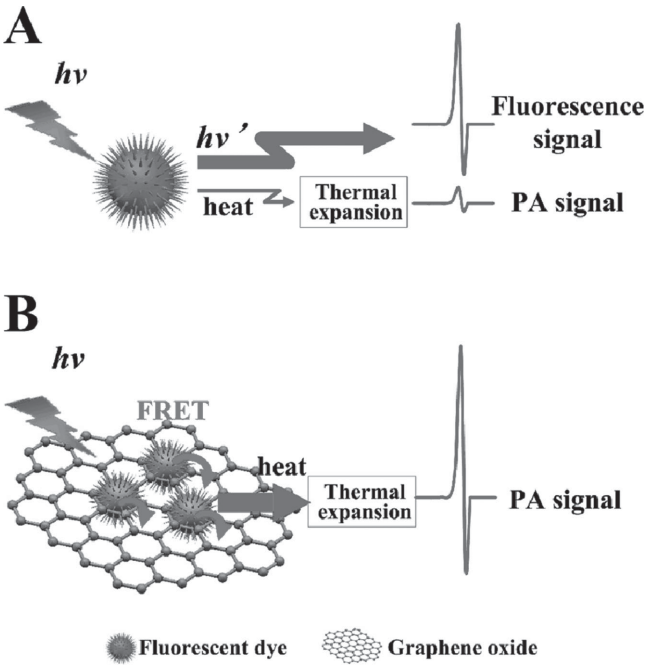

Figure 1. Characterization of PA enhancement process. A) Fluorescent dyes with strong absorption, strong fluorescence, and weak thermoelastic wave characteristics and B) π–π stacking of dyes in close proximity to GO. GO quenches the dye fluorescence via FRET between dye molecules and GO. Using the pulse laser irradiation, the vast majority of absorbed light energy is converted to acoustic waves.

Fluorescence quenching PA probes are easy to assemble and transform. They combine the advantages of dyes and GO, including the spectral absorption selectivity and stability of dyes as well as the biocompatibility of GO. Also, the fluorescence quenching nanoprobe absorption spectrum can be adjusted as required by attaching different dyes to GO. Other attractive features include their high mechanical flexibility and that they have no heavy metal ion-induced toxicity to living organisms, which is beneficial to their application in biomedicine.

In this study, fluorescence quenching nanoprobes were designed to enhance PAI tumor contrast and PA therapy efficiency. First, we demonstrated that GO quenches the attached dye fluorescence via FRET, resulting in higher PA signal than the sum of the separate signals generated in the dye and the GO. We then verified that the fluorescence quenching nanoprobe can enhance PA contrast of targets in deep-seated tissues and tumors in living mice. Finally, we measured the fluorescence quenching nanoprobes' PA therapy efficiency both in vitro and in vivo.

2. Results and Discussion

We constructed the fluorescence quenching probe (GO-dye) using GO and dyes via π–π stacking interactions (see Experimental Section for details).[45–50] GO, the base material of GO-dye, was utilized for loading dyes and quenching

DOI: 10.1002/smll.201403395

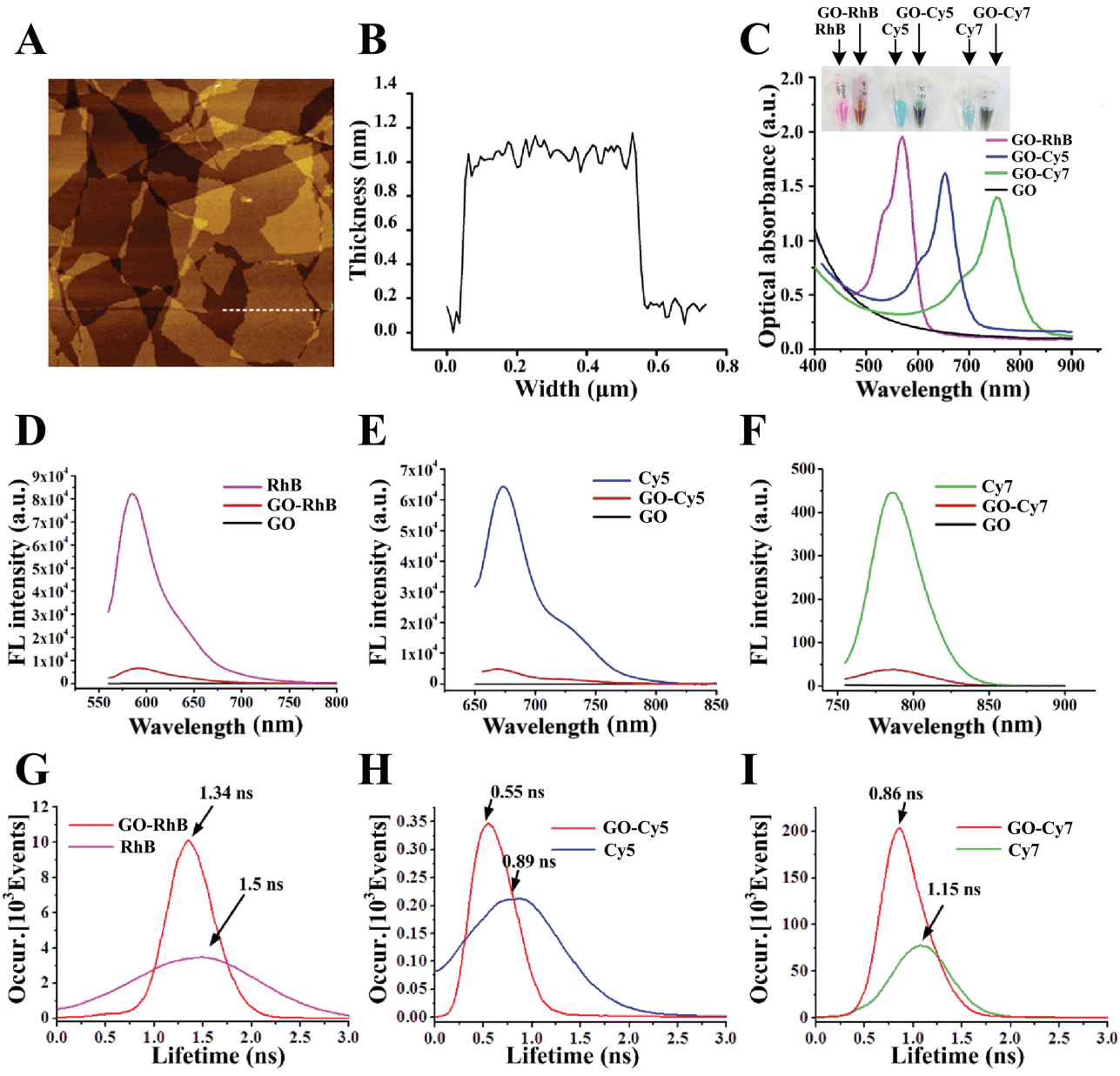

Figure 2. Characterization of GO-dyes. A) AFM image (size 2 × 2 μm²) of experimental GO. B) Depth profile of GO (dotted line in the A)). C) Optical absorption spectra of GO, GO–RhB, GO–Cy5, and GO–Cy7 and inset images of RhB, GO–RhB, Cy5, GO–Cy5, Cy7, and GO–Cy7 in the aqueous solution. D)–F) fluorescence (FL) spectra of GO, GO–RhB, RhB, GO–Cy5, Cy5, GO–Cy7, and Cy7. G)–I) Fluorescence lifetimes of RhB and GO–RhB, Cy5 and GO–Cy5, Cy7 and GO–Cy7.

dye fluorescence, while the dyes were utilized for selectively enhancing light energy absorption. GO morphology was detected by atomic force microscopy (AFM). Size was about 100–600 nm and the thickness was ≈1.2 ± 0.2 nm (**Figure 2**A,B). To demonstrate that multispectral PA probes for multispectral PAI application can be developed by loading different dyes on GO, rhodamine B (RhB), cyanine 5 (Cy5), and cyanine 7 (Cy7) were attached to GO, respectively. The absorption spectra of GO–RhB, GO–Cy5, and GO–Cy7 showed absorption peaks at 570, 654, and 753 nm, respectively (Figure 2C). GO-dye absorption at those peaks was significantly higher (8–14 times) at the same mass concentration than that of GO. As shown in the Figure 2C inset, GO–RhB, GO–Cy5, and GO–Cy7 were highly water-soluble and well-dispersed.

To demonstrate that the attached dye fluorescence can be quenched by GO via FRET, we measured the fluorescence intensities and lifetimes of dyes and corresponding GO-dyes. All dyes had showed strong fluorescence intensity in the aqueous solution. When we constituted the fluorescence quenching probe (GO-dye), the attached dyes' fluorescence intensities dropped significantly (Figure 2D–F). The lifetime measurements of dyes and GO-dyes are shown in Figure 2G–I. Lifetime measurements were performed using a Coherent Mira HP (high-power) system (wavelength range 700–1000 nm, pulse width 150 fs). The laser pulse repeat rate

DOI: 10.1002/smll.201403395

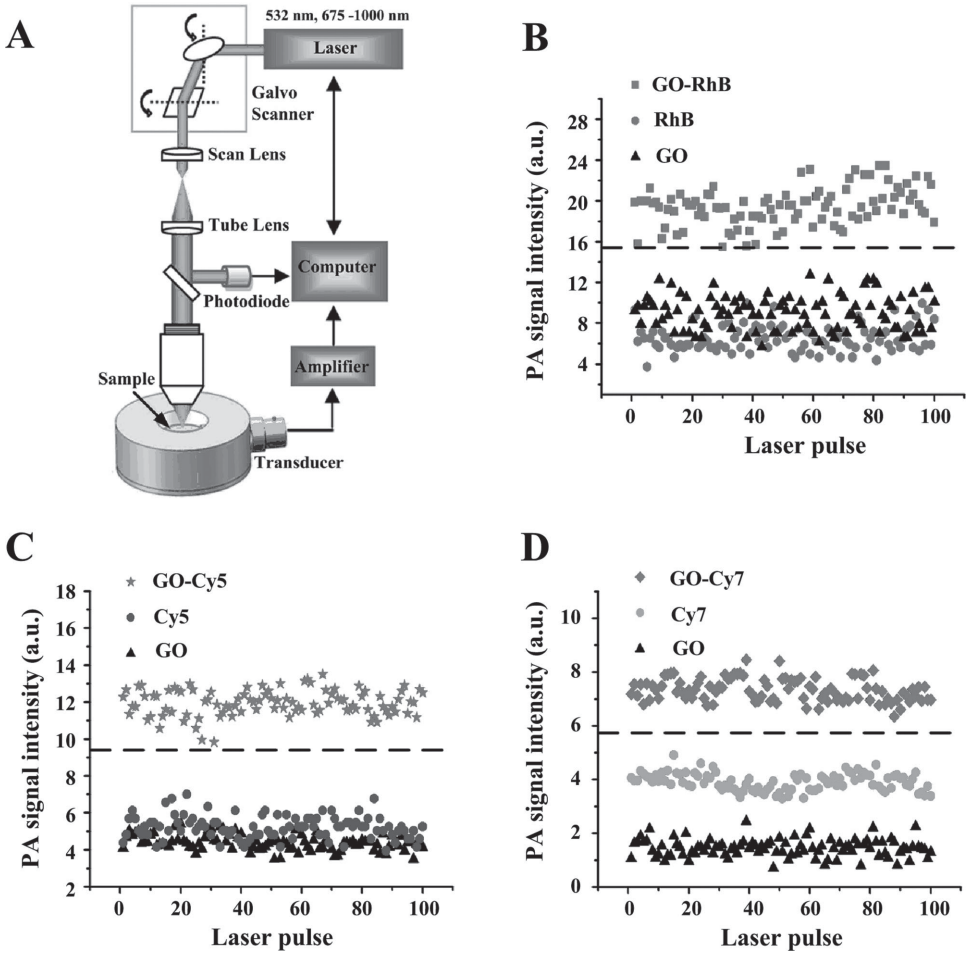

Figure 3. PA signal intensities of GO, dyes, and the corresponding GO-dyes. A) The schematic diagram of the experimental setup. B) PA signal intensities of RhB, GO, and GO–RhB at 532 nm; C) PA signal intensities of Cy5, GO, and GO–Cy5 at 675 nm; and D) PA signal intensities of Cy7, GO, and GO–Cy7 at 753 nm. Dotted lines in B), D), and F) indicate the sum of the separate measurements made in the dye solutions (RhB, Cy5, and Cy7) and GO particle suspension.

was 76 MHz, allowing a 13 ms time-window for measurement. The measured photon counts from the photomultiplier tube (PMT) and the chopper trigger signal were recorded simultaneously by a time-correlated single photon counter (TCSPC) (PicoQuant, NanoHarp 300). The lifetimes of the free dyes were 1.50, 0.89, and 1.15 ns, respectively. When dyes bonded to GO-forming GO-dyes, the three lifetimes decreased to 1.34, 0.55, and 0.86 ns, respectively. Considering the observed dyes' fluorescence quenching, their decreased lifetimes could be due to FRET between dye molecules and GO.[53,54]

To verify that fluorescence quenching can lead to PA signal enhancement, we measured the PA signal intensities of GO, RhB, Cy5, Cy7, GO–RhB, GO–Cy5, and GO–Cy7 using a PA microscopy system (**Figure 3**A). In the PA signal measurements experiment, the mass concentrations of GO and dyes were separately prepared and identical to the concentration of GO and dye that GO-dye particle suspensions contained. Under the same experimental parameters, the PA signal intensities of GO-dyes were higher than those of GO and dyes alone and even higher than the sum of the separate measurements made in the dye solutions and GO particle suspension (Figure 3B–D). The PA signals of the GO-dyes have increased 25.3%, 24.3%, and 23.7% compared with the sum of the separate measurements made in the dye (RhB, Cy5, and Cy7) solutions and GO suspension. The quantum efficiency of RhB, Cy5, and Cy7 was 0.31, 0.27, and 0.27 in aqueous solution, respectively. The PA signal increase is lower than that. This could be attributed to the dyes fluorescence being quenched incompletely. The high PA signal of GO-dye relative to the same concentration of the corresponding dye and GO is likely due to fluorescence quenching, making the absorbed light energy of fluorescent dyes mainly decay in a nonradioactive way as heat. The energy originally released in the form of fluorescence can convert to PA waves. We could conclude that the pulse laser energy absorbed by GO-dyes was mostly converted into heat via fluorescence quenching on FRET. The localized heating led to the rapid expansion and generation of acoustic pressure waves and thus ultimately improved the conversion of the absorbed laser energy to acoustic energy.

Currently, PAI has been used in tumor imaging in vivo.[12–14] The tissue light absorption between 650 and 950 nm is minimal, so deep tumor imaging is possible. GO–Cy7, with an absorption peak at 753 nm, was selected as the candidate fluorescence quenching probe to demonstrate the possibility of in vivo studies. The ability to detect

DOI: 10.1002/smll.201403395

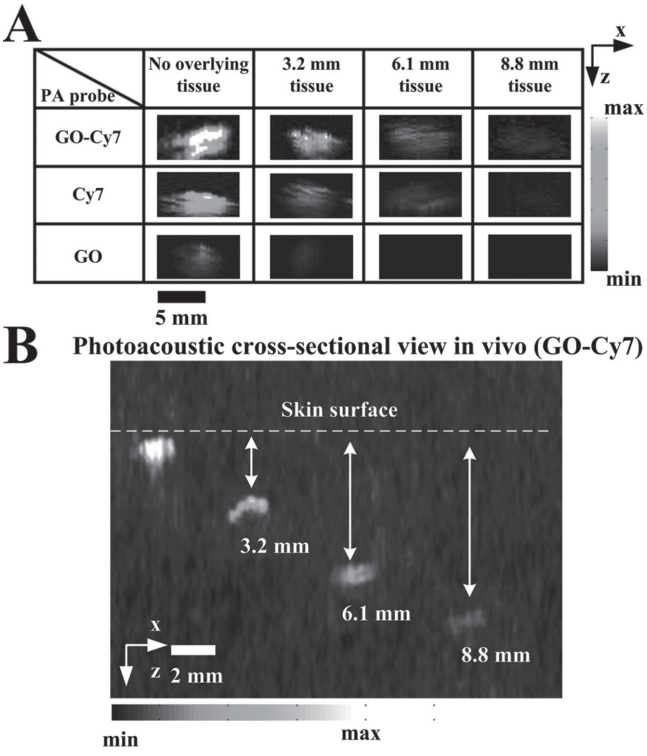

Figure 4. A) Tissue mimicking phantoms with inclusions containing GO, Cy7, and GO–Cy7, respectively, at increasing depths. B) PAI cross-sections of inclusions containing GO–Cy7 at increasing depths in the rabbit leg in vivo.

the GO–Cy7 PA signal in living subjects was tested with subcutaneous agar-containing solution injections ranging in concentration from 4.28 to 68.48 μg mL^{-1} into mice dorsal areas (Figure S1A, Supporting Information). Linear correlations between concentration and PA signal were observed (Figure S1B, Supporting Information). The GO–Cy7 limit of detection in living mice was ≈4.28 μg mL^{-1}. To demonstrate that GO–Cy7 can enhance higher PAI contrast in deep-seated tissue compared to Cy7 and GO, we subcutaneously injected GO–Cy7, Cy7, and GO inclusions (mixed with 2%-agar) into mouse backs. We then imaged them with overlaying chicken breast tissue to imitate different depths. Under the equivalent excitation energy, GO–Cy7 can effectively generate higher PA contrast than GO and Cy7 (**Figure 4**A). This was attributed to its higher optical-acoustic conversion efficiency compared to Cy7 and higher extinction coefficient compared to GO. To demonstrate that GO–Cy7 can enhance PA contrast in deep tissue in vivo, we obtained PA imaging in different deep tissue regions of the rabbit leg in vivo after injecting GO–Cy7 (mixed with 2%-agar, 21.4 μg mL^{-1}). The GO–Cy7 sample, with a 21.4 μg mL^{-1} concentration, can be detected up to 8.8 mm deep in the tissue (Figure 4B). The results suggested that GO–Cy7 has the potential to enhance the PAI contrast of deep-seated targets beyond the limits of modern pure optical imaging systems.

To selectively enhance PAI tumor contrast, targeted GO–Cy7 can be constructed by conjugating integrin $\alpha_v\beta_3$ mAb on carboxylated GO (GO–Abs/Cy7). Integrin $\alpha_v\beta_3$ is overexpressed on U87-MG cell cytomembranes. We observed no obvious changes in the three probes' fluorescence and absorption characteristics (data not shown). First, we studied the GO–Abs/Cy7 biodistribution in mice. Considering the fluorescence of the attached Cy7 on GO was quenched, the additional Cy7 conjugated to integrin $\alpha_v\beta_3$ mAb and formed GO–Abs–Cy7/Cy7 for fluorescence imaging. We sacrificed U87-bearing Balb/c nude mice before injection and at 1, 6, and 24 h postinjection. The main organs and tumor tissues were spectrally imaged by the ODYSSEY Infrared Imaging System (LI-COR, Inc., Lincoln, NE) (**Figure 5**A). H: heart, LU: lung, LI: liver, K: kidney, SP: spleen, ST: stomach, and T: tumor. The averaged Cy7 fluorescent intensity of each imaged organ (after removing the tissue autofluorescence and subtracting the background of each organ before GO–Abs–Cy7/Cy7 injection) was calculated for a semiquantitative biodistribution analysis (Figure 5B). A strong fluorescent signal was observed in tumors and reticuloendothelial systems, including the liver and spleen. GO–Abs–Cy7/Cy7 levels in most organs decreased over time as expected. Second, inflammatory response after intravenous administration of GO–Abs/Cy7 was tested. The concentrations of cytokines (interleukin-1β(IL-1β) and tumor necrosis factor-α(TNF-α)) in the serum were determined using commercially available enzyme-linked immunosorbent assay (ELISA) kits (Multisciences). All the steps are followed the specifications of manufacturer. Balb/c mice were treated with GO–Abs/Cy7 at doses of 2.7 mg kg^{-1} and without GO–Abs/Cy7 as control. Balb/c mice were sacrificed after treatment of 24 h and experiments were performed using three samples. The proinflammatory cytokines were increased after intravenous administration of GO–Abs/Cy7. In the treated group, IL-1β was increased to 6.75 ± 0.58 from 1.44 ± 0.12 pg mL^{-1} in control group. TNF-α was also increased to 10.86 ± 0.94 pg mL^{-1} in treated group from 3.82 ± 0.21 pg mL^{-1} in control group (Figure S2, Supporting Information).

We next sought to determine whether GO–Abs/Cy7 could be used for tumor detection in vivo. Mice bearing U87-MG tumors were divided into two groups (n = 3 mice per group). After validating that GO–Abs/Cy7 had no obvious toxicity in vitro and in vivo (Figure S3, Supporting Information), the first group was injected through the tail vein (IV) with 200 μL GO–Abs/Cy7 (including 107 μg mL^{-1} GO–Cy7). For the second group, separate GO–Abs (100 μL, including 200 μg mL^{-1} GO) and Cy7 (100 μL, 14 μg mL^{-1}) solutions were injected simultaneously into the same mice. The PA signals from a region of interest in the tumors in the two groups were measured. The PA signal was significantly higher in mice injected with GO–Abs/Cy7 compared with those injected with separate GO–Abs and Cy7 solutions simultaneously (**Figure 6**A). At 6 h postinjection of GO–Abs/Cy7, the PA signal increased by ≈130%, from 31 ± 2.9 to 69 ± 6.5 AU(arbitrary unit), while in mice injected with GO–Abs and Cy7, the PA signal only increased by 42% (Figure 6B). These results demonstrated that GO–Abs/Cy7 can enhance the PAI tumor contrast more than separately injected GO–Abs and Cy7 solutions. GO–Abs/Cy7 could thus be used for tumor detection in vivo.

PA therapy using probes as "acoustic bomb" agents is a newly developed approach in cancer therapy.[13–15]

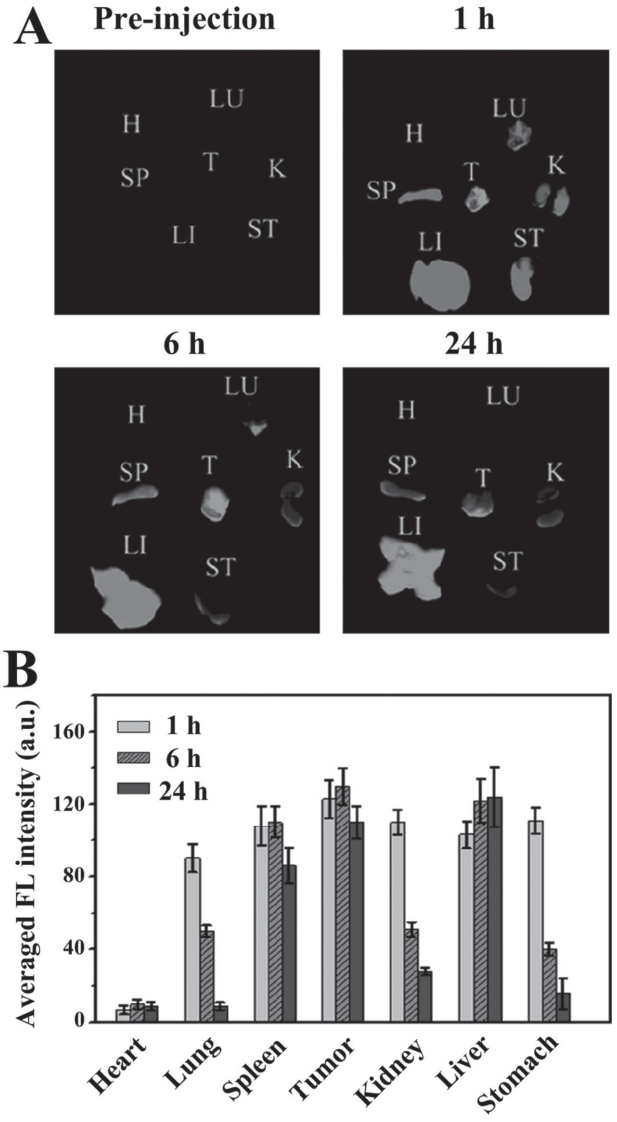

Figure 5. Semiquantitative biodistribution analysis of GO–Abs–Cy7/Cy7. Considering the fluorescence of the attached Cy7 on GO was quenched, the additional Cy7 conjugated to integrin $\alpha_v\beta_3$ mAb, forming GO–Abs–Cy7/Cy7 for fluorescence imaging. A) U87-bearing Balb/c nude mice were sacrificed before injection and at 1, 6, and 24 h postinjection. The main organs and tumor tissues were spectrally imaged by the ODYSSEY Infrared Imaging System (LI-COR, Inc., Lincoln, NE). H: heart, LU: lung, LI: liver, K: kidney, SP: spleen, ST: stomach, and T: tumor. B) The averaged Cy7 fluorescent intensity of each imaged organ (after removing the tissue autofluorescence and subtracting the background of each organ before GO–Abs/Cy7 injection) was calculated for a semiquantitative biodistribution analysis. The error bars represent standard error (n = 3 mice).

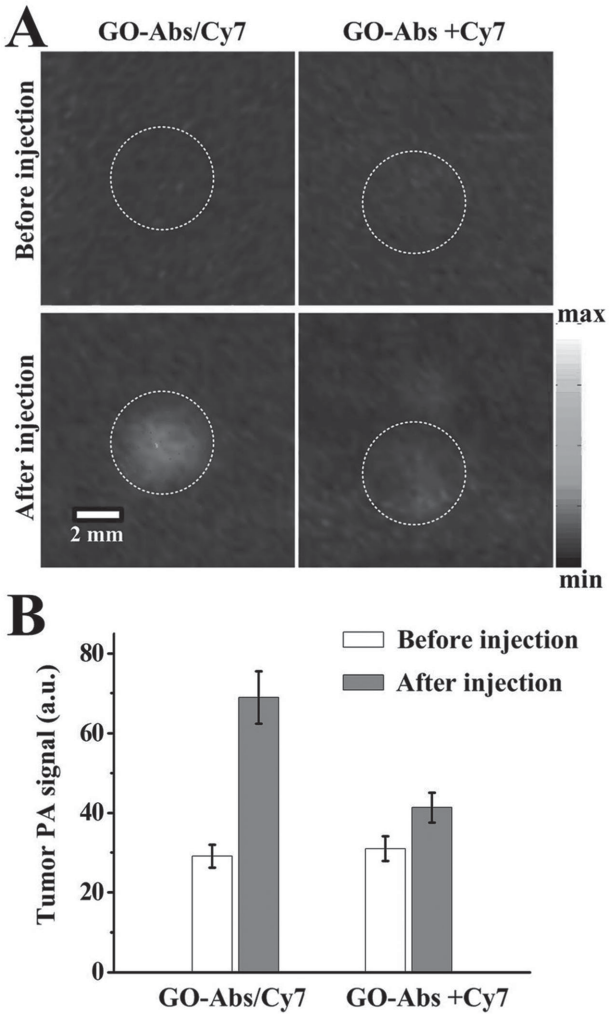

Figure 6. The comparison of PAI contrast of tumors after being injected with GO–Abs/Cy7, GO–Abs, and Cy7. A) The first group of U87-bearing Balb/c nude mice (n = 3) was injected through the tail vein (IV) with GO–Abs/Cy7 (the first row). In the second group (n = 3), separate GO–Abs and Cy7 solutions were injected simultaneously into the same mice (the second row). The PA images in the first line represent the mouse group before injection and the second line represents the mouse 6 h after being injected with GO–Abs/Cy7 or GO–Abs plus Cy7. The white dotted lines on the images illustrate the approximate tumor edges. B) Quantification of the signals in the tumor shows higher in the PA image after injecting GO–Abs/Cy7 compared to before injection and in the other group (the injection of GO–Abs and Cy7 in the same mouse). The error bars represent standard error (n = 3 mice).

GO–Abs/Cy7 with high optical-acoustic conversion will be an effective candidate for PA therapy. To determine the PA effect of GO–Abs/Cy7 on cells, we measured cell viability after different U87-MG cell treatments. GO–Abs/Cy7 cytotoxicity depended on its concentration as well as the irradiation laser energy. Cells treated with 16 mJ cm^{-2} of laser irradiation and GO–Abs/Cy7 (GO–Cy7 concentrations ranging from 10.7 to 21.4 μg mL^{-1}) showed significant cytotoxicity (**Figure 7**A,B). To investigate the destructive effect of GO–Abs/Cy7 under laser irradiation on U87-MG cells, we detected cell morphology. After being treated with GO–Abs/Cy7 plus laser irradiation, cells became shrunken, loosely arranged, and did not gradually adhere well (Figure 7C). We then performed Hoechst 33258 staining to directly observe chromatin condensation, an indication of apoptosis. The results indicated that GO–Abs/Cy7 plus pulse laser irradiation could induce U87-MG cell apoptosis (Figure 7D). GO–Abs/Cy7 has potential for application in PA therapy.

To further elucidate that GO–Abs/Cy7 is a high-effect tumor cell killing agent in deep-seated tissues, cell apoptosis induced by different treatments was analyzed by flow cytometry with annexin V-fluorescein isothiocyanate (FITC)/Propidium Iodide (annexin-V/PI) double staining assay. After

DOI: 10.1002/smll.201403395

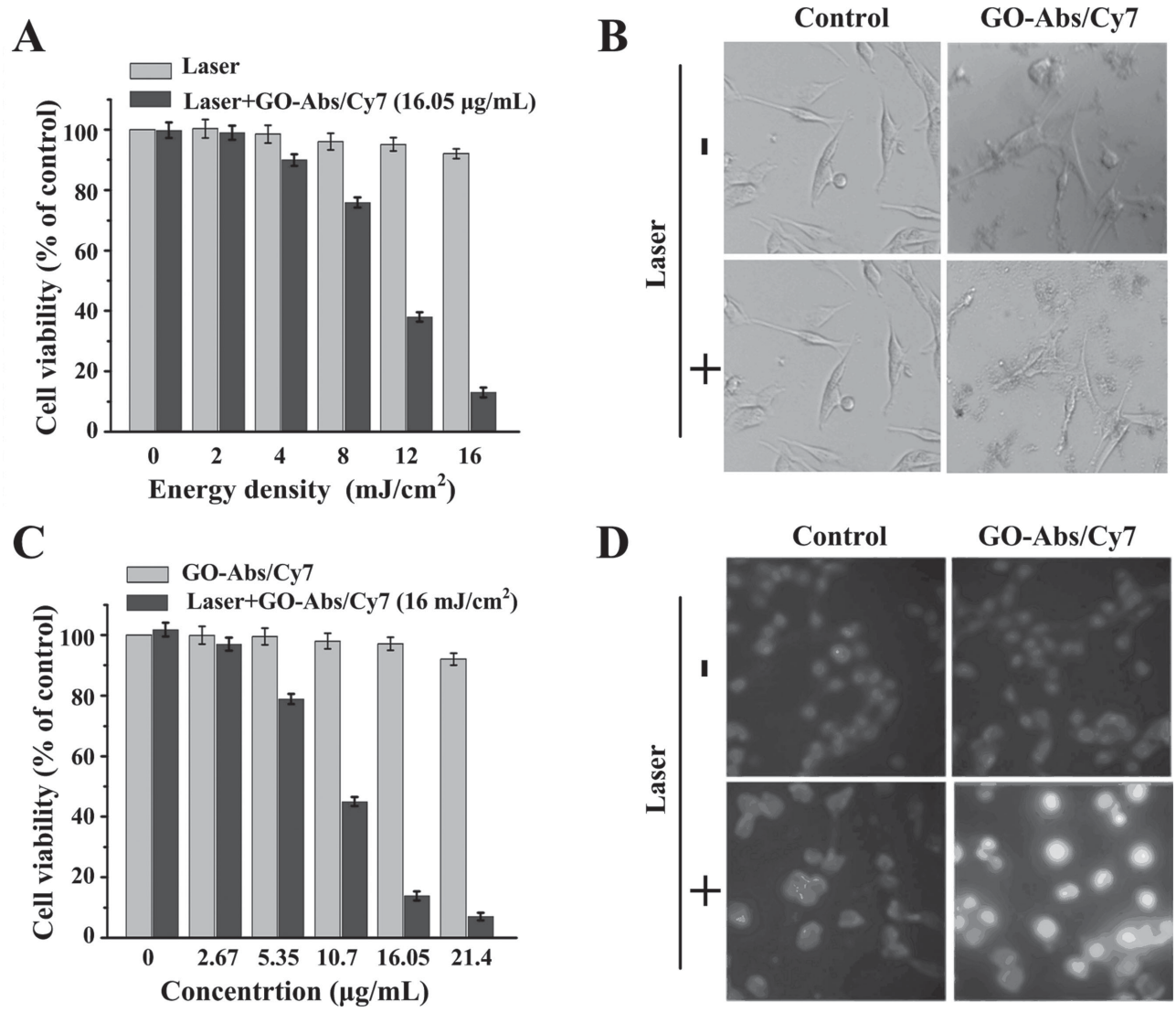

Figure 7. PA effect of GO–Abs/Cy7 on U87–MG cell death. A) At different laser energy (2–16 mJ cm^{-2}); B) At different GO–Abs/Cy7 concentrations ranging from 10.7 to 21.4 μg mL^{-1}; C) Optical images of U87-MG cells incubated with GO–Abs/Cy7 before and after laser irradiation; D) Hoechst 33258 morphological examination of apoptosis in U87-MG cells. Cells were incubated with GO–Abs/Cy7 for 2 h, irradiated by a pulse laser, and finally incubated in complete medium for 30 min before assessing cell viability. Cells without any treatment were used as control. The error bars represent standard error ($n = 4$).

2 h of incubation with GO–Abs/Cy7 (including 16.05 μg mL^{-1} GO–Cy7), GO–Abs (including 15 μg mL^{-1} GO), Cy7–Abs (including 1.06 μg mL^{-1} Cy7), and SWNTs–Abs (including 15 μg mL^{-1} SWNTs), respectively, the U87-MG cells with chicken breast tissue (thickness of 3.2 mm) overlays were irradiated by a pulsed laser at 753 nm (on the chicken breast tissue surface, the laser energy density is 80 mJ cm^{-2}; 60 s). As expected, laser irradiation plus GO–Abs/Cy7 obviously induced cell death, as shown by the stronger positive annexin V–FITC signal compared to that in cells treated with laser irradiation plus GO-Abs, Cy7-Abs, or SWNTs-Abs (**Figure 8**). The killing efficiency of GO-Abs/Cy7 was higher than GO-Abs, Cy7-Abs, or SWNTs-Abs. The strong laser-induced wave from GO-Abs/Cy7 can effectively induce U87-MG cell apoptosis, and with its high efficiency at killing cancer cells, it could be used for PA therapy in deep-seated tissue.

After the in vitro experiments, we finally examined GO–Abs/Cy7's tumor cell killing effects in vivo. U87-MG cells were injected subcutaneously in the flanks of female Balb/c nude mice. When the tumor size reached ≈50 mm^3, the animals were divided into various treatment groups ($n = 10$). We intravenously injected 200 μL GO–Abs/Cy7 (217 μg mL^{-1}) solutions. In this injection dose, GO–Cy7 concentrations in the tumor were estimated, reaching up to 25 μg mL^{-1} (Figure S4, Supporting Information). This concentration is high enough to allow for PA therapy. Six hours after intravenous injection with GO–Abs/Cy7, we used a single laser pulse at 753 nm, with a laser fluence of ≈20 mJ cm^{-2} and a pulse repetition rate of 20 Hz (60 s), for PA therapy. To determine tumor cytotoxicity of the PA effect with GO–Abs/Cy7, scathe levels in tumors were examined after PA therapy using terminal deoxy-nucleotidyl transferase dUTP nick end labeling (TUNEL) staining (30 min after PA therapy) and H&E

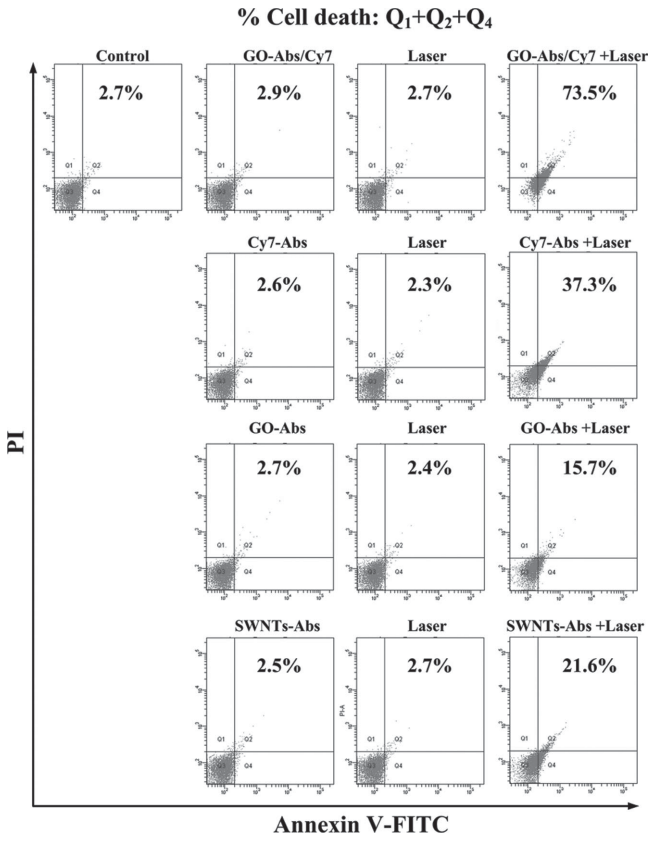

Figure 8. The comparison of efficiency of tumor cell death in deep-seated tissue by GO–Abs/Cy7 plus laser irradiation, GO–Abs plus laser irradiation, Cy7–Abs plus laser irradiation, and SWNTs–Abs plus laser irradiation. Analysis of apoptosis in differently treated U87-MG cells was performed by flow cytometry with annexin-V/PI double staining assay.

staining (1 day after PA therapy). A high scathe level was observed in the cells treated by laser plus GO–Abs/Cy7 compared to the control group (**Figure 9**A,B). After treatment, mice were observed daily, and the tumor volumes were measured using a caliper every other day. Laser plus GO–Abs/Cy7 treatment in mice significantly suppressed tumor growth compared to laser plus GO–Abs and laser plus Cy7–Abs, as well as the control group (Figure 9C). The tumor volumes in laser plus GO–Abs/Cy7 treatment groups were significantly smaller than that in other groups from the beginning of treatment to the end of the experiment (Figure 9C). Moreover, the survival time of mice treated with laser plus GO–Abs/Cy7 was longer than those treated with laser plus GO–Abs, laser plus Cy7–Abs, and the control group (Figure 9D). Altogether, we observed a marked antitumor effect of PA therapy with laser plus GO–Abs/Cy7 in vivo, resulting in decreased tumor growth and prolonged survival time.

Generally, nanoparticles or dye molecules release absorbed light energy in two ways: radiative transition (photon) and nonradiative transition (heat). The relationship between the two consists of one falling and the other rising. The PA wave generation energy only comes from nonradiative energy. Quenching fluorescence is one way to increase the proportion of nonradiative energy. GO-dyes enhance the proportion of nonradiative energy via FRET to quench dye fluorescence, which ultimately enhances optical-acoustic conversion efficiency. This method may convert existing fluorescent dyes into high-efficiency PA probes.

The method of enhancing the probe absorption coefficient for PA signal enhancement is certainly important. However, this method needs new materials to enhance the probe's absorption coefficient, and developing new materials will use more time and energy. Conversely, fluorescence quenching PA probes are composed of GO and commercial dyes. This type of probe is easy to assemble and transform. It combines the advantages of dyes and GO, including the spectral absorption selectivity and stability of dyes and the biocompatibility of GO. Fluorescence quenching PA probes have good practicability and are easy to apply for PA tumor imaging as well as PA tumor therapy in vivo.

There are two reasons that GO is chosen rather than SWNTs as the base material of fluorescence quenching PA probes. First, GO's specific surface area is bigger compared to SWNTs. The bigger surface area allows more dyes to bind to GO for enhancing absorption in its unit mass. Second, GO quenches dye fluorescence via FRET, which is dependent upon the spatial orientation of the proposed acceptor and donor. It is likely the planar structure of GO that enables a better spatial orientation compared to SWNTs.[55] Hence, GO has higher quenching efficiency than carbon nanotubes, a conclusion verified by our experiment (Figure S5, Supporting Information).

The size of GO may influence the PA and targeting effects. Larger GO with larger surface area can load more dyes to enhance light absorbance, ultimately generated stronger PA signal in one nanoparticle. However, GO nanosheets with large and small size are taken up by cells predominantly through phagocytosis and clathrin-mediated endocytosis, respectively.[56] It means that the larger GO may preferentially translocate into the reticuloendothelial system, resulting in reduced tumor targeting efficiency. Tumor targeting efficiency of smaller GO will be better than that of large GO due to that smaller GO are endocytosed less by reticuloendothelial system.[57,58] The suitable size of GO served as a base material for loading dyes needs to be further optimized to compose PA nanoprobes with high optical-acoustic conversion efficiency and targeting efficiency.

In recent years, many kinds of molecules were immobilized on GO for in vivo imaging or therapy via the π–π stacking interaction.[59–62] The interactions between these molecules and GO are stable under pH 7.4, and most of the molecules can be delivered to the targeted sites by GO in vivo. However, some molecules would be released from GO under the acidic condition slowly (less than 20%).[63,64] In our study, Cy7 was bound on GO through the π–π stacking interaction as well. Considering our in vitro experimental results (Figure S6, Supporting Information), in vivo PA tumor imaging results (Figure 6) and other research groups' results, we estimated that most of the Cy7 molecules would still bound on GO surface during the in vivo blood circulation. In next step, some conjugation approaches will be utilized to improve the integrity of the therapeutic system, such as covalent linkages.

Photothermal therapy is a therapeutic strategy in which photon energy is converted into heat to damage and destroy cancer cells with continuous laser radiation. While

DOI: 10.1002/smll.201403395

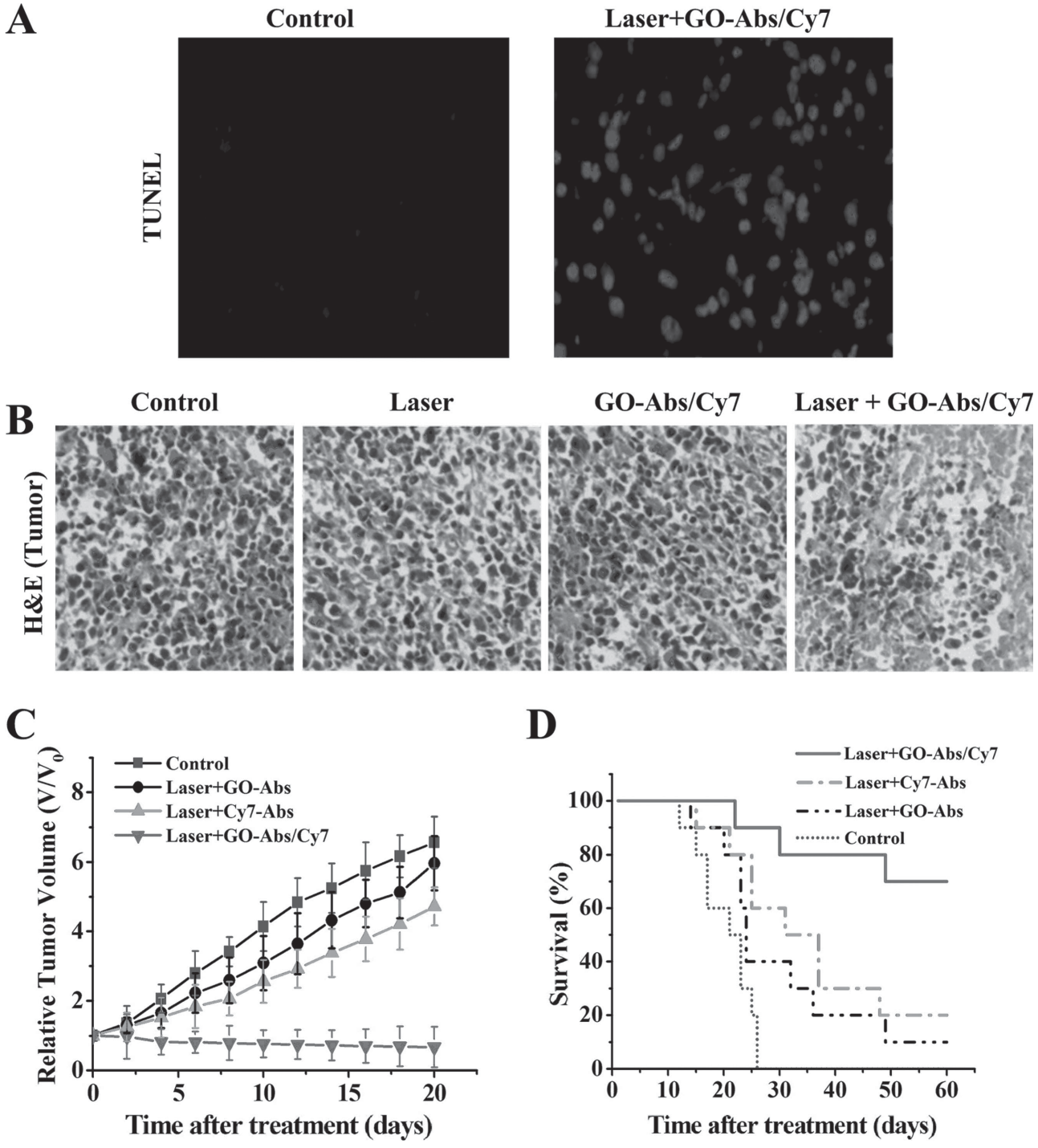

Figure 9. PA effect of GO–Abs/Cy7 on tumor therapy in vivo. A) Apoptosis detection in tumors by fluorometric TUNEL analysis. Tumors were harvested 30 min after light exposure in the GO–Abs/Cy7 treatment group. Only apoptotic cells were stained green with fluorescein conjugated TUNEL. B) Relative volumetric change in tumor size of various treatment groups (GO–Abs/Cy7, GO–Abs, and Cy7–Abs). V_0 was the tumor volume at the time of laser treatment ($n = 10$). Error bars indicate standard deviations. C) Survival rate in different treatment groups ($n = 10$).

PA therapy utilizes photoinduced acoustic shockwave (PA wave) to destroy cancer cells.[13–15] Heat conduction is very low in the PA therapy (Figure S7, Supporting Information) because the duration of the laser pulse (4–6 ns) is much shorter than the thermal diffusion time (submicrosecond).[65] Based on the PA effect, the PA wave to destroy cancer cells is produced inside the absorber by the thermal expansion that results from a small temperature rise, which is caused by the absorption of externally applied radiation of pulsed laser.[1,2]

Both PAI and PA therapy are based on the PA effect. The difference between them is that the excitation energy utilized for PA therapy is much higher than for PAI. The fluorescence quenching PA probe described here could apply to both PAI and PA therapy. PAI is a relatively new technique

DOI: 10.1002/smll.201403395

that allows deeper tumors to be imaged with higher spatial resolution compared to most optical techniques. After quantifying energy thresholds utilized in PAI and PA therapy, we can institute an integrated diagnosis and therapy protocol: PAI can detect orthotopic tumors in deep-seated tissue and provide tumor location information. Subsequently, PA therapy is regionally selectively implemented with the guidance of PAI. The high surface area of GO-dyes allows the loaded anticancer drugs to be delivered to the cancer lesion location. PAI, PA therapy, and chemotherapy methods can be combined in this novel nanoplatform and serve as a powerful hybrid method in both diagnosis and therapy.

3. Conclusion

In conclusion, we have reported a novel fluorescence quenching PA probe with highest availability of optical-thermo conversion. In vitro and in vivo tests show that the fluorescence quenching PA probes have minimal toxicity. We successfully utilized this probe to selectively enhance PAI tumor contrast and PA therapy efficiency in vivo. This new PA probe could be an effective multifunctional probe for deep-seated tumor imaging and therapy in vivo.

4. Experimental Section

Materials: GO dispersion solution was purchased from Nanjing XF Nano Materials Tech Co. Ltd. (Nanjing, China). Rhodamine B was purchased from Sigma Company (USA). Cy5 and Cy7 were purchased from Bridgen biotechnology Co. Ltd (Beijing, China). SWNTs were obtained from Chinese Academy of Sciences (Cheng du, China). Since all the chemicals were analytical grade and were used without further purification. The high-purity deionized water (resistance >18 MΩ cm) is used throughout. U87-MG human glioblastoma cancer cells were obtained from the Cell Culture Center of SunYat-sen University (Guangzhou, China). Female BALB/c nude mice (age: 4–5 weeks; bodyweight: 16–18 g) were obtained from Center of Experimental Animals at SunYat-sen University. Animal procedures were in agreement with the guidelines of the Institutional Animal Care and Use Committee. The mice that were detected in the PA system were fully anesthetized.

Preparation of GO-Dyes: The π–π interaction is a noncovalent interaction resulting from the negative charge transferring from a π system to another π system, when one of the systems is electron-rich and the other electron-deficient. The dyes were bound with GO via π–π interactions between their π systems. The GO-dye nanoprobes were prepared by adding Rhodamine B, Cy5, and Cy7 into phosphate buffer saline (PBS) of GO, respectively. After stirring for 2 h, the unattached dyes were removed by being centrifuged at 13 000 rpm for 10 min. The fluorescence of the supernatant was measured using the LS-55 fluorescence spectrophotometer (Perkin-Elmer, USA). In the GO-dye particle suspensions, the final mass concentrations are 224 μg mL^{-1} for GO–RhB solution containing 200 μg GO and 24 μg RhB in 1 mL, 217 μg mL^{-1} for GO–Cy5 solution containing 200 μg GO and 17 μg Cy5 in 1 mL, 214 μg mL^{-1} for GO–Cy7 solution containing 200 μg GO and 14 μg Cy7 in 1 mL.

Preparation of Tumor-Targeted GO–Cy7, Cy7, GO, and SWNTs: Integrin $\alpha_v\beta_3$ monoclonal antibody was bounded to Cy7,carboxylated GO, and SWNTs by the covalently linkage of carboxyl groups with amino groups, with 1-ethyl-3-[3-dimethylaminopropyl]carbodiimide hydrochloride (EDC) and N-hydroxy succinimide (NHS) to accelerate the reaction.

Characterization Experiments: Tapping mode AFM (Agilent 5500AFM) purchased from Agilent Technologies, Inc. (Englewood, USA) was used for detecting the surface characterization of GO. The AFM samples were prepared by casting 5–10 μL (0.2 mg mL^{-1}) of GO aqueous solution on mica plate. The morphology of GO was characterized by AFM, which also showed the thickness of GO was ≈1.2 ± 0.2 nm.

The optical absorbance characteristic of GO, GO–RhB, GO–Cy5, and GO–Cy7 was investigated by UV/visible absorption spectra (Lambda-35 UV/visible spectrophotometer, Perkin-Elmer, MA, USA). Fluorescence spectra of GO, GO–RhB, GO–Cy5, GO–Cy7, RhB, Cy5, and Cy7 were investigated by an LS-55 fluorescence spectrophotometer (Perkin-Elmer). Lifetime measurements were performed using a Coherent Mira HP system (wavelength range 700–1000 nm, pulse width 150 fs). The laser pulse repeat rate was 76 MHz, allowing a 13 ms time-window for measurement. The measured photon counts from the PMT and the chopper trigger signal were recorded simultaneously by a TCSPC (PicoQuant, NanoHarp 300).

PA signal intensities of GO, GO–RhB and RhB, GO–Cy5 and Cy5, GO–Cy7 and Cy7 solution were measured by PA microscopy system. The excitation wavelengths were 532 nm for GO–RhB and RhB, 675 nm for GO–Cy5 and Cy5, and 753 nm for GO–Cy7 and Cy7, respectively. The experimental setup was shown in Figure 4A. A tunable pulsed laser with a repetition rate of 20 Hz and a pulse width of 4 ns (neodymium-doped yttrium aluminium garnet (Nd:YAG) Surelight-II-20 connected to Surelite optical parametric oscillator (OPO) Plus, Spectral tuning range 675–1000 nm, Continuum) was used as the light source. The light through galvo mirrors, scan lens, and tube lens was then focused by the objective lens to irradiate the tested samples. The average energy density of the laser at the wavelengths used in this study was set to about 6 mJ cm^{-2} at the target site. The transducer (Doppler Electronic Technologies Co., Ltd., China) with center frequency of 10 MHz and –6 dB bandwidth of 100% was used to receive the PA signals generated by the tested samples. The PA signals were recorded by the computer through the signal amplifier and a dual-channel data acquisition card. The sampling rate of the data acquisition card was 200 Msamples s^{-1}. A silicon photodiode (ET 2000, Electro-Optics Technology, Inc., Traverse City, USA) was used to monitor and calibrate the intensity and stability of the laser beam.

Cell Culture: U87 MG human glioblastoma cancer cells in Eagle's minimal essential medium. The media were supplemented with 10% fetal bovine serum and 1% penicillin–streptomycin, in 5% CO_2, 95% air at 37 °C in a humidified incubator.

Cellular Toxicity by CCK8 Assay: Cytotoxicity in vitro was examined with a colorimetric tetrazolium salt-based assay using a Cell Counting Kit-8 (CCK8, Dojindo Laboratories, Kumamoto, Japan). To detect cytotoxicity, tumor cells were irradiated by the pulse laser at energy of 2–16 mJ cm^{-2} with or without GO–Cy7 incubation. Then the absorbance of each well at 450 nm was measured by Infinite M200 (TECAN, Mannedorf, Switzerland). The results were expressed as the mean percentage of cell viability relative to untreated cells.

Cell Apoptosis Assay: For analysis of apoptosis by nuclear staining, cell apoptosis was morphologically evaluated with Hoechst 33258. U87-MG human glioblastoma cancer cells were

DOI: 10.1002/smll.201403395

treated as indicated and incubated for 2 h in 35-mm dishes. Hoechst 33258 (10 mg mL^{-1}) was added to each dish and the cells were incubated at 37 °C with 5% CO_2 for an additional 30 min in the dark. Fluorescence images of the normal and apoptotic cells were examined with a modified commercial microscope system equipped with a mercury lamp (band-pass filter 352–461 nm), a 395 nm dichroic mirror, and a long-pass filter 397 nm emission filter (LSM510/ConfoCor2; Zeiss, Jena, Germany). The fluorescence images were collected via a Zeiss C-Apochromat objective (40×, NA 1.3). Quantification of apoptosis by annexin V/PI staining was performed as described previously. Apoptotic cell death was determined using the BD ApoAlert annexin V–FITC apoptosis kit (Becton–Dickinson Biosciences, Mountain View, CA, USA) according to the manufacturer's instructions. Flow cytometry was performed on a BD FACSCanto II flow cytometer (Becton–Dickinson).

PA Therapy: Six hours after intravenous injection with 200 µL GO–Abs/Cy7 (including 214 µg mL^{-1} GO–Cy7), a single laser pulse at 753 nm with a laser fluence of ≈20 mJ cm^{-2} and a pulse repetition rate of 20 Hz (60 s) was used for in vivo PA therapy. Then, the mice were observed daily and the tumor volumes were measured using a caliper every other day.

PA Microscopy System: The experimental setup was shown in Figure S8, Supporting Information. A tunable pulsed laser with a repetition rate of 20 Hz and a pulse width of 4 ns (Nd:YAG Surelight-II-20 connected to Surelite OPO Plus, Spectral tuning range 675–1000 nm, Continuum) was used as the light source. The light through galvo mirrors, scan lens, and tube lens, then was focused by the objective lens to irradiate the tested samples. The average energy density of the laser at the wavelengths used in this study was set to be ‹20 mJ cm^{-2} at the target site. The ultrasonic transducer ((Doppler Electronic Technologies Co., Ltd., China)) with center frequency of 10 MHz and –6 dB bandwidth of 100% was used to receive the PA signals generated by the tested samples. The PA signals were recorded by the computer through the signal amplifier and a dual-channel data acquisition card. The sampling rate of the data acquisition card was 200 Msamples s^{-1}. A 3D scanning stage was driven by computer-controlled stepper motors (MC600AS, Zolix). A silicon photodiode (ET 2000, Electro-Optics Technology, Inc., Traverse City, USA) was used to monitor and calibrate the intensity and stability of the laser beam.

Deep-Tissue PAI System: In the deep-tissue PAI system (Figure S9, Supporting Information), a tunable pulsed laser with a repetition rate of 20 Hz and a pulse width of 4 ns (Nd:YAG Surelight-II-20 connected to Surelite OPO Plus, Spectral tuning range 675–1000 nm, Continuum) was used as the light source. The laser passed through a slit aperture and focused, using a cylindrically focusing lens, onto the sample, creating a planar sheet of light. The incident energy density on the tissue surface was set at ‹20 mJ cm^{-2}. The 128-element linear transducer was used for PA signal acquisition. The multielement transducer has a center frequency of 2.5 MHz with a nominal bandwidth of 70%.

Supporting Information

Supporting Information is available from the Wiley Online Library or from the author.

Acknowledgements

This research is supported by the National Basic Research Program of China (2011CB910402 and 2010CB732602), and the National Natural Science Foundation of China (61361160414, 61331001, and 81127004), and the Guangdong Natural Science Foundation (S2013020012646). The authors thank Professor Xunbin Wei of Shanghai Jiao Tong University for revising the paper.

[1] M. Xu, L. V. Wang, *Rev. Sci. Instrum.* **2006**, *77*, 041101.
[2] L. V. Wang, S. Hu, *Science* **2012**, *335*, 1459.
[3] V. Ntziachristos, D. Razansky, *Chem. Rev.* **2010**, *110*, 2783.
[4] X. Wang, Y. Pang, G. Ku, X. Xie, G. Stoica, L. V. Wang, *Nat. Biotechnol.* **2003**, *21*, 803.
[5] H. Zhang, K. Maslov, G. Stoica, L. V. Wang, *Nat. Biotechnol.* **2006**, *24*, 848.
[6] R. I. Siphanto, K. K. Thumma, R. G. M. Kolkman, T. G. Leeuwen, F. F. M. Mul, J. W. Neck, L. N. A. Adrichem, W. Steenbergen, *Opt. Express* **2004**, *13*, 89.
[7] Y. Lao, D. Xing, S. Yang, L. Xiang, *Phys. Med. Biol.* **2008**, *53*, 4203.
[8] E. I. Galanzha, E. V. Shashkov, P. M. Spring, *Cancer Res.* **2009**, *69*, 7926.
[9] D. Razansky, D. Distel, C. Vinegoni, R. Ma, N. Perrimon, R. W. Koster, V. Ntziachristos, *Nat. Photonics* **2009**, *3*, 412.
[10] S. Yang, D. Xing, Q. Zhou, L. Xiang, Y. Lao, *Med. Phys.* **2007**, *34*, 3294.
[11] M. Li, J. Oh, X. Xie, G. Ku, W. Wang, C. Li, G. Lungu, G. Stoica, L. V. Wang, *Proc. IEEE* **2008**, *96*, 481.
[12] S. Shriram, J. H. Amirian, S. H. Litovsky, R. W. Smalling, S. Y. Emelianov, *Opt. Express* **2008**, *16*, 3362.
[13] B. Kang, D. Yu, Y. Dai, S. Chang, D. Chen, Y. Ding, *Small* **2009**, *11*, 1292.
[14] F. Zhou, S. Wu, Y. Yuan, W. R. Chen, D. Xing, *Small* **2012**, *10*, 1543.
[15] J. Zhong, S. Yang, X. Zheng, T. Zhou, D. Xing, *Nanomedicine (London, U. K.)* **2013**, *8*, 903.
[16] M. Eghtedari, A. Oraevsky, J. A. Copland, N. A. Kotov, A. Conjusteau, M. Motamedi, *Nano Lett.* **2007**, *7*, 1914.
[17] M. F. Kircher, A. de la Zerda, J. V. Jokerst, C. L. Zavaleta, P. J. Kempen, E. Mittra, K. Pitter, R. M. Huang, C. Campos, F. Habte, R. Sinclair, I. K. M. Brennan, E. C. Holland, S. S. Gambhir, *Nat. Med.* **2012**, *18*, 829.
[18] A. de la Zerda, S. Bodapati, R. Teed, S. Y. May, T. S. M. abakman, Z. Liu, B. T. Khuri-Yakub, X. Chen, H. Dai, S. S. Gambhir, *ACS Nano* **2012**, *6*, 4694.
[19] A. de la Zerda, Z. Liu, S. Bodapati, R. Teed, S. Vaithilingam, B. T. Khuri-Yakub, X. Chen, H. Dai, S. S. Gambhir, *Nano Lett.* **2010**, *10*, 2168.
[20] W. J. Akers, C. Kim, M. Berezin, K. Guo, R. Fuhrhop, G. M. Lanza, G. M. Fischer, E. Daltrozzo, A. Zumbusch, X. Cai, L. V. Wang, S. Achilefu, *ACS Nano* **2011**, *5*, 173.
[21] Y. Chen, W. Frey, S. Kim, P. Kruizinga, K. Homan, S. Emelianov, *Nano Lett.* **2011**, *11*, 348.
[22] B. Wang, E. Yantsen, T. Larson, A. B. Karpiouk, S. Sethuraman, J. L. Su, K. Sokolov, S. Y. Emelianov, *Nano Lett.* **2009**, *9*, 2212.
[23] E. I. Galanzha, E. V. Shashkov, T. Kelly, J. W. Kim, L. Yang, V. P. Zharov, *Nat. Nanotechnol.* **2009**, *4*, 855.
[24] K. Yang, L. Hu, X. Ma, S. Ye, L. Cheng, X. Shi, C. Li, Y. Li, Z. Liu, *Adv. Mater.* **2012**, *24*, 1868.
[25] H. Qin, T. Zhou, S. H. Yang, Q. Chen, D. Xing, *Nanomedicine (London, U. K.)* **2013**, *8*, 1611.
[26] L. Nie, M. Chen, X. Sun, P. Ronga, N. Zheng, X. Chen, *Nanoscale* **2014**, *6*, 1271.
[27] L. Nie, S. Wang, X. Wang, P. Rong, A. Bhirde, Y. Ma, G. Liu, P. Huang, G. Lu, X. Chen, *Small* **2014**, *10*, 1585.

DOI: 10.1002/smll.201403395

[28] D. Razansky, C. Vinegoni, V. Ntziachristos, *Opt. Lett.* **2007**, *32*, 2891.
[29] Y. Zhang, X. Cai, Y. Wang, C. Zhang, L. Li, S. Choi, L. V. Wang, Y. Xia, *Angew. Chem.* **2011**, *123*, 7497.
[30] Y. Wang, X. Xie, X. Wang, G. Ku, K. L. Gill, D. P. O'Neal, G. Stoica, L. V. Wang, *Nano Lett.* **2004**, *4*, 1689.
[31] X. Yang, S. E. Skrabalak, Z. Li, Y. Xia, L. V. Wang, *Nano Lett.* **2007**, *7*, 3798.
[32] A. De La Zerda, C. Zavaleta, S. Keren, S. Vaithilingam, S. Bodapati, Z. Liu, J. Levi, B. R. Smith, T. J. Ma, O. Oralkan, Z. Cheng, X. Y. Chen, H. J. Dai, B. T. Khuri-Yakub, S. S. Gambhir, *Nat. Nanotechnol.* **2008**, *3*, 557.
[33] G. Ku, M. Zhou, S. Song, Q. Huang, J. Hazle, C. Li, *ACS Nano* **2012**, *6*, 7489.
[34] K. Song, C. L. Kim, C. M. Cobley, Y. Xia, L. V. Wang, *Nano Lett.* **2009**, *9*, 183.
[35] K. Pu, A. J. Shuhendler, J. V. Jokerst, J. G. Mei, S. S. Gambhir, Z. Bao, J. Rao, *Nat. Nanotechnol.* **2014**, *9*, 233.
[36] L. Boucharda, M. S. Anwarb, G. L. Liuc, B. Hannc, Z. H. Xie, J. W. Grayc, X. D. Wang, A. Pines, F. F. Chen, *Proc. Natl. Acad. Sci. USA* **2009**, *106*, 4086.
[37] C. Wang, C. Bao, S. Liang, H. Fu, K. Wang, M. Deng, Q. Liao, D. Cui, *Nanoscale Res. Lett.* **2014**, *9*, 264.
[38] C. Bao, N. Beziere, P. del Pino, B. Pelaz, G. Estrada, F. Tian, V. Ntziachristos, J. M. de la Fuente, D. Cui, *Small* **2013**, *9*, 68.
[39] S. Link, C. Burda, M. B. Mohamed, B. Nikoobakht, M. A. El-Sayed, *J. Phys. Chem. A* **1999**, *103*, 1165.
[40] S. Link, B. Burda, B. Nikoobakht, M. A. El-Sayed, *J. Phys. Chem. B* **2000**, *104*, 6152.
[41] C. M. Aguirre, C. E. Moran, J. F. Young, N. J. Halas, *J. Phys. Chem. B* **2004**, *108*, 7040.
[42] P. R. Selvin, *Nat. Struct. Biol.* **2000**, *7*, 730.
[43] Z. Chen, S. Berciaud, C. Nuckolls, T. F. Heinz, L. E. Brus, *ACS Nano* **2010**, *4*, 2964.
[44] G. Gomez-Santos, T. Stauber, *Phys. Rev. B* **2011**, *84*, 1.
[45] H. Dong, W. Gao, F. Yan, H. Ji, H. Ju, *Anal. Chem.* **2010**, *82*, 5511.
[46] J. Kim, L. J. Cote, F. Kim, J. Huang, *J. Am. Chem. Soc.* **2010**, *132*, 260.
[47] V. Georgakilas, M. Otyepka, A. B. Bourlinos, V. Chandra, N. Kim, K. C. Kemp, P. Hobza, R. Zboril, K. S. Kim, *Chem. Rev.* **2012**, *112*, 6156.
[48] K. S. Kim, S. B. Suh, J. C. Kim, B. Hong, E. C. Lee, S. Yun, P. Tarakeshwar, J. Y. Lee, Y. Kim, H. Ihm, H. G. Kim, J. W. Lee, J. K. Kim, H. M. Lee, D. Kim, C. Cui, S. J. Youn, H. Y. Chung, H. S. Choi, C. W. Lee, S. J. Cho, S. Jeong, J. H. Cho, *J. Am. Chem. Soc.* **2002**, *124*, 14268.
[49] I. Geronimo, E. C. Lee, N. J. Singh, K. S. Kim, *J. Chem. Theory Comput.* **2010**, *6*, 1931.
[50] W. Wang, P. Hobza, *ChemPhysChem* **2008**, *9*, 1003.
[51] K. A. Mkhoyan, A. W. Contryman, J. Silcox, D. A. Stewart, G. Eda, C. Mattevi, S. Miller, M. Chhowalla, *Nano Lett.* **2009**, *9*, 1058.
[52] C. Gomez-Navarro, R. T. Weitz, A. M. Bittner, M. Scolari, A. Mews, M. Burghard, K. Kern, *Nano Lett.* **2007**, *7*, 3499.
[53] H. S. S. Ramakrishna Matte, K. S. Subrahmanyam, K. V. Rao, S. J. George, C. N. R. Rao, *Chem. Phys. Lett.* **2012**, *50*, 2987.
[54] R. S. Swathi, K. L. Sebastian, *J. Chem. Phys.* **2008**, *129*, 054703.
[55] E. Morales-Narvaez, B. Perez-Lopez, L. Baptista Pires, A. Merkoci, *Carbon* **2012**, *50*, 2987.
[56] Q. Mu, G. Su, L. Li, B. O. Gilbertson, L. H. Yu, Q. Zhang, Y. P. Sun, B. Yan, *ACS Appl. Mater. Interfaces* **2012**, *4*, 2259.
[57] K. Yang, S. Zhang, G. Zhang, X. Sun, S. T. Lee, Z. Liu, *Nano Lett.* **2010**, *10*, 3318.
[58] X. Hu, J. Hu, J. Tian, Z. Ge, G. Zhang, K. Luo, S. Liu, *J. Am. Chem. Soc.* **2013**, *135*, 17617.
[59] B. Tian, C. Wang, S. Zhang, L. Feng, Z. Liu, *ACS Nano* **2011**, *5*, 7000.
[60] P. Rong, K. Yang, A. Srivastan, D. O. Kiesewetter, X. Yue, F. Wang, L. Nie, A. Bhirde, Z. Wang, Z. Liu, G. Niu, W. Wang, X. Chen, *Theranostics* **2014**, *4*, 229.
[61] Z. Liu, J. T. Robinson, X. Sun, H. Dai, *J. Am. Chem. Soc.* **2008**, *130*, 10876.
[62] L. Zhang, J. Xia, Q. Zhao, L. Liu, Z. Zhang, *Small* **2010**, *6*, 537.
[63] X. Sun, Z. Liu, K. Welsher, J. T. Robinson, A. Goodwin, S. Zaric, H. Dai, *Nano Res.* **2008**, *1*, 203.
[64] X. Yang, Y. Wang, X. Huang, Y. Ma, Y. Huang, R. Yang, H. Duan, Y. Chen, *J. Mater. Chem.* **2011**, *21*, 3448.
[65] T. Sun, G. J. Diebold, *Nature (London)* **1992**, *355*, 806.

Received: November 14, 2014
Revised: December 22, 2014
Published online:

DOI: 10.1002/smll.201403395